Gas Flow Patterns in Horizontal Epitaxial Reactor Cells Observed by Interference Holography

L. J. Giling

Faculty of Science, R.I.M. Department of Solid State III, Catholic University, Toernooiveld, Nijmegen, The Netherlands

ABSTRACT

Interference holography is used to visualize gas flow patterns and temperature profiles in epitaxial systems. It is demonstrated that in water-cooled horizontal reactor cells the carrier gases H_2 and He give dynamically stable laminar flow profiles throughout the reactor. There is no indication of a stagnant or boundary layer for flow velocities up to 80 cm/sec in this type of cell. In air-cooled cells, H_2 and He also give stable laminar flow profiles, but beyond velocities of 40 cm/sec a cold gas finger appears in these flows due to undeveloped flow and temperature profiles. In contrast to the stable flow characteristics of H_2 and He, the flows of N_2 and Ar always are unstable due to convective motions. Besides this intrinsic instability, these flows are accompanied by severe entrance effects (especially undeveloped flow profiles), which dominate the flows for flow rates higher than 4 cm/sec. This is observed for both air- and water-cooled cells. Another phenomenom which is observed for N_2 and Ar is that beyond 4 cm/sec the convective gas breaks up into a thin (8 mm) laminar layer close to the susceptor across which the entire temperature gradient is present and a highly turbulent/convective part above this laminar layer. Analysis shows that for Ar and N_2 about eight times longer entrance lengths in the reactor cell are needed to achieve fully developed velocity and temperature profiles as compared with H_2 and He. This explains the dominant influence of this effect on the flows of Ar and N_2. When the influence of the entrance effect on the profiles is taken into account, all the observed flow patterns and temperature gradients are in agreement with the theoretical flows which can be predicted on basis of the respective Reynolds and Rayleigh (or Grashof) numbers.

Although chemical vapor deposition of silicon is widely used, the flow characteristics and the temperature profiles inside the epitaxial reactor are still a point of discussion. The system which is best studied in this connection is the horizontal epitaxial reactor cell. For this type of cell Eversteijn *et al.* (1, 2) studied the flow pattern of a stream of hydrogen in a horizontal water-cooled reactor by looking at the streamlines of a smoke of TiO_2, obtained from $TiCl_4$ and H_2O. From these experiments Eversteijn developed the stagnant layer model in which an immobile thin layer of gas of a few millimeters thickness was assumed to be present just above the heated susceptor. Ban (3, 4), in addition to flow visualization experiments with TiO_2 smoke, measured temperature profiles with a moving thermocouple, while concentration measurements were performed by mass analysis. He concluded that the flows and temperatures in an air-cooled reactor were complicated by entrance effects. Sedgwick (5) determined temperature and concentration profiles by means of Raman scattering. He also used an air-cooled reactor and came to the conclusion that temperature profiles did depend on the position along the susceptor. In addition a steep temperature gradient was measured above the susceptor.

The flow situation in a horizontal epitaxial reactor is complicated by the fact that the gas, which enters the reactor cell with a rather high flow velocity, suddenly hits a hot susceptor. This means that the total resultant flow will be affected by: (*i*) the possibility of turbulence due to the high flow velocities, (*ii*) the occurrence of convection as a result of buoyancy forces, and (*iii*) the presence of entrance effects because the flow and temperature profiles have to develop to their final profiles. How much these separate effects will contribute to the final flow pattern will depend on the process parameters such as cell design, flow velocities, nature of the gases, temperature, etc.

Viewed in that light, it would indeed be advantageous to know at the outset how these flows would look like for any particular combination of gases, reactor cell, and temperature. The above-mentioned observation methods are not really suited to give this kind of information. However, an interesting additional technique for the study of temperature profiles and flow patterns in a gaseous system is given by the method of interference holography. In this technique and in one single experiment, a complete survey is obtained of both the temperature distribution and the flow pattern over the entire epitaxial reactor cell. The real power of the method lies in the ability to observe gas flows in real time. This possibility makes the method very attractive for the study of flow and temperature profiles. This can be done for various gases, flow velocities, susceptor temperatures, and various cell designs. The feasibility of this method was put forward at the International Conference on Crystal Growth (ICCG) V in Boston (6).

In this paper emphasis will be given to the flow patterns of the gases H_2, He, Ar, and N_2 in water and air-cooled reactor cells at various flow velocitites and susceptor temperatures. A quantitative analysis of the temperature profiles will be the subject of a forthcoming paper.

Key words: boundary layer, entrance effects, laminar flow, turbulent flow, convection.

The Technique of Interference Holography

Interference holography is one of the main applications of holography. It is used to study vibration patterns on mechanical systems, but it is also well suited to detect density fluctuations in gases. For general information on this subject the reader is referred to the books of Collier and DeVelis (7, 8).

The method in principle is based upon normal interference between two coherent light beams. However, the fundamental difference with usual interference, where two beams combine at one time and one place, is that in interference holography the original and second beam are separated in time, the first beam is recorded by a photographic plate, the modified second beam is added to this exposure (technique of double exposure), or is mixed in with the reconstructed first beam (real time). Here the developed hologram serves to generate the original light beam at the proper time. The experimental setup for interference holography is depicted schematically in Fig. 1. The light beam of a laser is split up into a reference beam and a sample beam, and both are combined again at a photographic plate which stores the amplitude and phase information. For real time holography the photographic plate is developed; this process produces an amplitude or absorption hologram. When this now transparent hologram is placed back into its original position and is

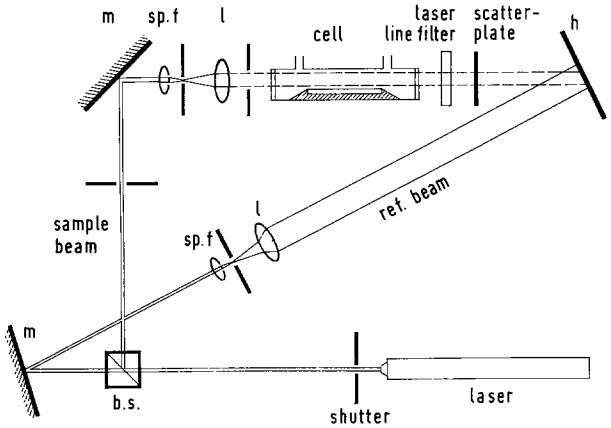

Fig. 1. Schematic diagram of a holographic system: b.s. = beam splitter, m = mirror, sp.f. = spatial filter, l = lens, h = hologram.

exposed with the reference beam only, the transmitted beam is forced to vibrate according to the pattern which is present on the hologram, resulting in a reconstruction of the original beam behind the hologram (Fig. 2). In interference holography this reconstructed beam is mixed with a slightly modified sample beam, which will result in interference phenomena, and because the original sample beam is frozen in the hologram and can be reproduced at will, this reconstructed beam can serve as a permanent reference frame. This means that when the reproduced original sample beam is compared with the modified sample beam, changes in real time can be observed between both states of the system.

The requirements for the successful application of this method are: (*i*) The developed hologram should be exactly repositioned at its original place to guarantee that the reconstructed beam indeed is generated at its original position; and (*ii*) the modified sample beam and the reconstructed beam must be coherent. The first requirement can be met by developing the photographic plate *in situ*, or after normal development, by careful piezoelectrical repositioning. The second requirement is met by splitting a laser beam into a sample and reference beam with the same lengths in light paths. It must be noted here that the reference beam now serves to reconstruct the original sample beam, whereas during the first exposure it was needed to register the phase of the sample beam.

The other way to observe changes in the sample is the technique of double exposure. Here the photographic plate is exposed two times, first before and then after the modification of the object. After development and repositioning in its original place, both recorded states will be reproduced when the plate is exposed with the reference beam. An interference pattern will occur behind the plate wherever there are light path differences between the two reconstructed beams. A significant advantage of this method is that the plate is not removed from its position between the two exposures, so in principle the method is more accurate than the previously mentioned method of real time. In addition no expensive plateholder is needed, because an exact repositioning of the hologram to its original position is not necessary. A very important disadvantage is that only a momentary picture of the changing object is obtained and that more time is involved in mapping a complete sequence of changes.

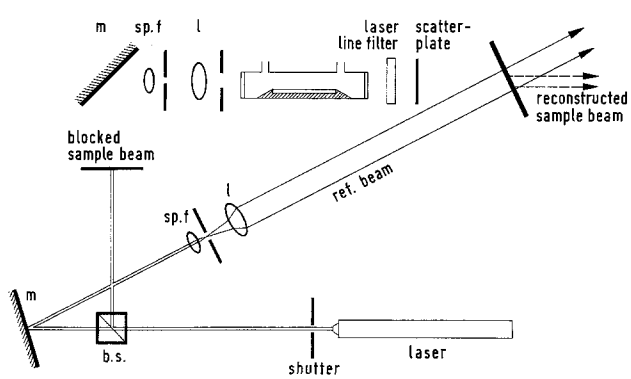

Fig. 2. Reconstruction of original sample beam behind developed hologram. When the sample beam is also allowed to go through, then behind the hologram two beams are mixed: the real sample beam and the reconstructed sample beam. This gives lead to interference.

Application of Interference Holography for the Visualization of Flow Patterns

In an epitaxial reactor cell a carrier gas flows over a graphite susceptor (Fig. 3). When no heating is applied, the gas is at room temperature (300 K) and throughout the cell the density of the gas is the same. At a distance z normal to the susceptor the optical path l_1 in the x-direction over the length L of the susceptor is given by

$$l_1 = \int_L n_{300} dx$$

the integral value of which is independent of the z-coordinate when the temperature and thus the refractive index n is constant throughout the cell. When the susceptor is heated, the temperature of the gas will rise to a value $T(z)$. In that case the light path at the same z-position is given by

$$l_2 = \int_L n_T dx$$

The difference in light paths between the two situations is then given by

$$\Delta l = \int_L (n_{300} - n_T)\, dx$$

and constructive and destructive interference will occur for $\Delta l = m\lambda$ and $\Delta l = (m + \frac{1}{2})\lambda$, respectively, in which m is a discrete number. The resultant interference pattern will consist of a large number of fringe lines and because of the one to one relation between refractive index and temperature each fringe also is a line of constant temperature (isotherm). So by counting the number of fringes and by measuring the positions, the temperature can be calculated all over the cross section of the reactor cell. This will be worked out in more detail in the next paper.

In this paper we will focus attention on the flow pattern of the streaming gas obtained for different carrier gases in various reactors. The parameters used are flow velocity and temperature. In these experiments we have the problem that the connection between the observed interference fringes and the actual flow pattern is not clear immediately. In principle it can be said that when the gas stream is stable and is

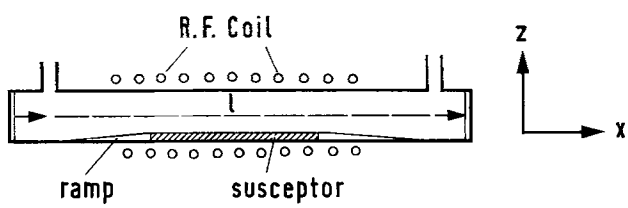

Fig. 3. Expitaxial reactor cell fitted with optical end windows for flow visualization experiments. The graphite susceptor is heated by rf coupling.

laminar, the temperature profile will be stable leading to a fixed fringe pattern in time, but when there is convection the temperature will follow the streamlines which then will show up as moving fringes. When the gas is highly turbulent and well mixed, the local temperatures will rapidly change and the fringe pattern will become blurred. Especially with real time observations one immediately discriminates between laminar, convective, and turbulent motions. This may be difficult with double exposures because in that technique short exposure times are used which may freeze in a convective or turbulent motion when these gas motions are slower than the exposure times.

Another problem is associated with the integration of the optical effect over the length of the cell. As we are mainly interested in the character of the flow over the susceptor, the contributions to the optical effect of the flows in the regions before and behind the susceptor should be kept minimal. Because the interference pattern is the result of a comparison of the optical lengths of the "sampling" state with a reference state, the contributions of both sections will be minimal when the temperature (*i.e.*, refractive index and density) of the gas in these regions is as close as possible to the reference temperature. The inlet region will give the smallest contribution, because the (room) temperature of the gas in this section will only be slightly affected by the radiation of the susceptor, especially because of the constant fresh supply of cold gas. It even does not matter whether the character of the gas flow will change from laminar to turbulent or vice versa in this section, as long as the temperature (*i.e.*, refractive index) of the reference state and sampling state are equal in both situations.

Analogous arguments hold for the end region. Here the contribution is expected to be larger, especially for air-cooled cells where the gas is not cooled by a water jacket. The effect is minimized by keeping this end section as short as possible compared to the length of the susceptor. Because the character of the flow in this end region will be of the same nature as that of the gas over the susceptor, in no case will a qualitative significant change of the resultant fringe pattern be expected. Only when the gas flow is laminar over the susceptor and suddenly, by some odd reason, becomes turbulent in the end region, a complete misinterpretation of the flow pattern as obtained from the fringe pattern can be the result.

A quantitative check as to whether both regions contribute significantly can be made for water-cooled cells. For a given susceptor length, one can calculate the number of fringes which should be present in the interference pattern as a result of the difference in (known) susceptor temperature and temperature of the water-cooled wall. In no cases studied were more fringes counted than theoretically predicted, indicating that the integrated length never significantly exceeded the real susceptor length. In other words, both end effects are unimportant, at least for water-cooled cells.

In principle it is possible to correct for both end effects by subtracting two double exposures made with the same end zones, but different susceptor lengths. This was done for a number of experiments, but no consistent set of data was obtained because the total accuracy appeared to be too low. The length of the susceptor was limited by the power of the rf generator to a maximum of 25 cm, whereas for accurate results a difference measurement should be done between two susceptors of 40 and 20 cm, respectively, in order to double the number of fringes.

If one neglects the effects of the regions before and behind the susceptor, then in principle it is also possible, by a correct analysis of the fringe pattern, to determine the local character of the flow over the length of the susceptor. By comparing this with the pattern for a fully developed flow, one can deduce the state of development of the flow along the susceptor.

Experimental

A horizontal epitaxial reactor cell fitted with optical end windows was placed in the sample beam of a holographic arrangement as depicted in Fig. 1. The cell was of the open-end type and was operated at 1 bar. Air-cooled and water-cooled cells were used with rectangular and circular cross sections. The overall inner length was 40-45 cm with free inner cross sections of about 8-11 cm^2. The free heights above the susceptor amounted to 20-29 mm depending on the type of reactor cell being used. Susceptors were made of graphite dimensions $20 \times 3.0 \times 1.0$ cm^3 for the circular and $20 \times 4.1 \times 0.5$ for the rectangular cells. In some experiments 10 or 15 cm long susceptors were used. The susceptors were provided with silica ramps on both sides in order to keep the gas flow as smooth as possible. No tilt was given to the susceptor. The susceptor was heated by means of a 4.5 kW rf generator which could give a maximum temperature of 1600 K in N_2 or Ar and about 150° lower in H_2 and He. The temperature was measured by a calibrated optical pyrometer. Because the flow pattern and temperature distribution is mainly determined by the carrier gases, pure carrier gases H_2, He, Ne, and Ar were used in the experiments. The input velocities were measured with calibrated flow meters.

The whole equipment was placed on an optical table provided with air cushions. Care was taken that the rf coil did not touch the reactor cell. All the optical components and the table itself were covered with aluminum foil in order to avoid heating up, and thus expansion, of the equipment. No solution was found for the presence of some convection of air in the optical path at both ends of the cell due to warming up of the air by the radiation. This effect was especially present with air-cooled cells and long operation times. It caused some slight trembling of the interference pattern, but it did not really affect the observations. An opaque glass window was placed between the cell and holographic plate. This plate collected all the light of the sample beam and acted as a scattering center. It also served as a fixed focusing point for the camera when photographs or films were made for documentation. For double exposures a laser line filter was used behind the cell in order to block the infrared radiation of the susceptor during the exposure of the hologram. Exposure times strongly depended on the power of the laser, on the sensitivity of the photographic plates and on the light loss by the optical components. Good holograms were obtained with exposure times of 1/15-1/100 sec using AGFA 10E75 plates and an He/Ne laser of 15 mW ($\lambda = 6328$A). Photographs of the real time observations were made with shutter times between 1/25 and 1/1000 sec.

Results

H_2 and He in a cylindrical air-cooled cell.—Typical results obtained with H_2 in an air-cooled circular reactor cell at two velocities are given in Fig. 4 and 5. A number of rather parallel fringes near the susceptor and several curved fringes higher up can be observed (Fig. 4). The dark rectangular area at the bottom of the tube is the cross section of the susceptor. This fringe pattern is very stable and no changes in time are observed by looking with real time holography. At high flow velocities (*i.e.*, input velocities) closed concentric fringes appear, but the stability of the fringe pattern is not affected (Fig. 5). An analogous behavior was observed at higher temperatures. The circular fringes also became more dominant when shorter susceptor lengths were used. Nearly identical

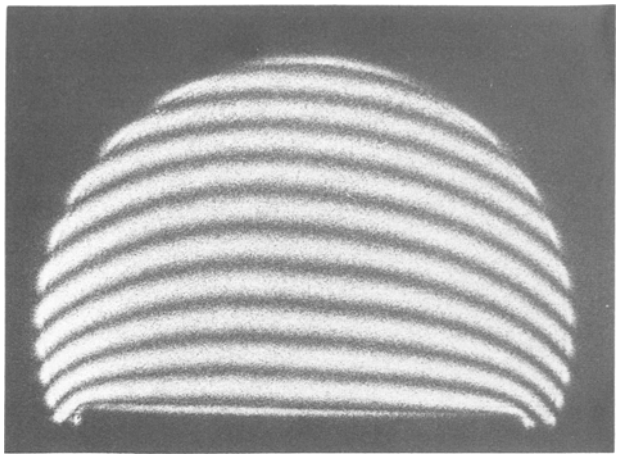

Fig. 4. H_2(He), low flow velocity $v = 10$ cm/sec. Air-cooled cylindrical cell, $T_{susc.} = 1350$ K, susceptor length = 20 cm. Note that the fringes end on the quartz wall of the reactor cell, which means that the wall is heated up by radiation of the susceptor.

phenomena are observed for helium as a carrier gas. Just as with H_2, helium also gave very stable fringe patterns at all flow velocities and temperatures, proving that also with He laminar flows are present. Also in this case closed concentric fringes appear at very high flow rates. Since the temperature dependence of the refractive index of He is smaller than for H_2, the number of fringes which can be observed with He is about four times smaller than for H_2. This makes He less attractive for accurate studies of the temperature distribution.

H_2 and He in a water-cooled cylindrical cell.—With a cylindrical water-cooled cell a fringe pattern as given in Fig. 6 is obtained. Also at higher flows hardly any changes in the fringe pattern can be observed. Even for flows up to 90 cm/sec, no concentric rings are formed; only a slight trembling of the fringes at the top is indicative of some disturbance. However, the bending of the fringes into the susceptor shows that for this kind of cell a strong temperature gradient is present across the surface of the susceptor.

N_2 and Ar in an air-cooled cylindrical reactor cell.—With N_2 and Ar, completely different fringe patterns are obtained. Figures 7-9 are typical for three situations which can be observed in an air-cooled cell. The pattern of Fig. 7 is obtained at very low flow velocities (<4 cm/sec). The pattern in itself is stable but shows three convective instability zones: two on both sides of the susceptor, one in the middle of the gas stream. By raising the flow beyond 4 cm/sec, the flow splits up

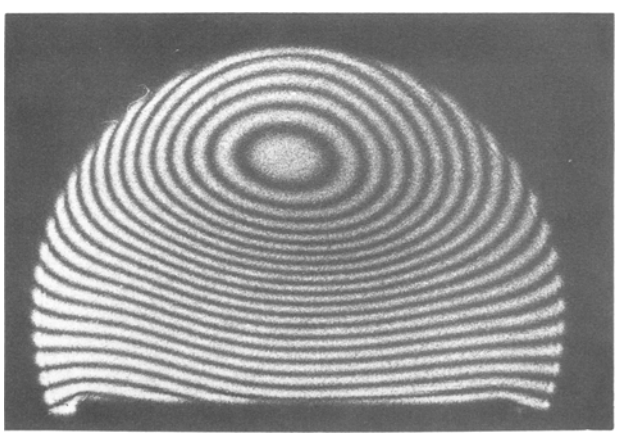

Fig. 5. H_2(He), high flow velocity $v = 70$ cm/sec. Air-cooled cylindrical cell, $T_{susc.} = 1350$ K, susceptor length = 20 cm.

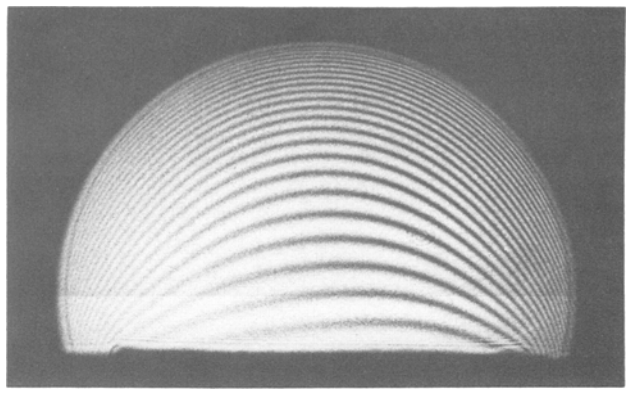

Fig. 6. H_2(He), all flow velocities $v \leq 90$ cm/sec (example 9.5 cm/sec.) Water-cooled cylindrical cell, $T_{susc.} = 1100$ K, susceptor length = 20 cm.

into a stable part with nearly parallel fringes near the susceptor and a thickness of about 8 mm and again a convective unstable part above it (Fig. 8). The instability mainly manifests itself by a movement of the closed rings from one side to the other at the same level. In addition, every few seconds a buoyant movement out of the stable laminar part was observed. At higher flows, *i.e.*, >10 cm/sec, the unstable upper part of the stream becomes more turbulent of character (Fig. 9). This turbulence causes local pressure differences on the top of the stable laminar layer. The result is that the thickness of the stable part locally varies

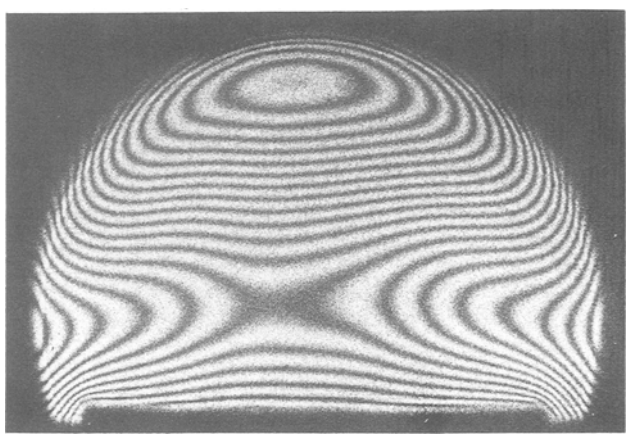

Fig. 7. N_2(Ar), low flow velocities $v \leq 4$ cm/sec (example 3 cm/sec). Air-cooled cylindrical cell, $T_{susc.} = 1300$ K, susceptor length = 20 cm.

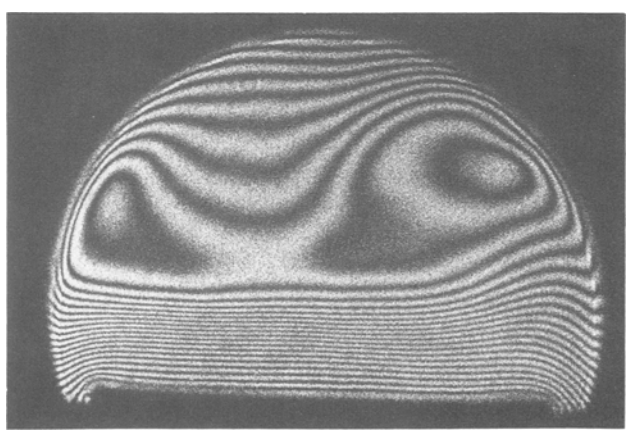

Fig. 8. N_2(Ar), medium flow velocities $4 \leq v \leq 10$ cm/sec (example 8 cm/sec). Air-cooled cylindrical cell, $T_{susc.} = 1350$ K, susceptor length = 20 cm.

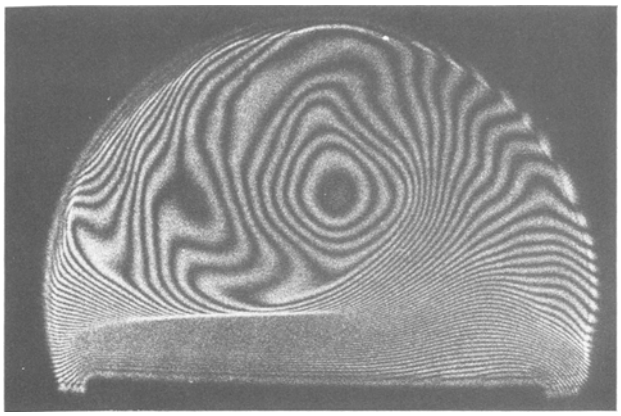

Fig. 9. N_2 (Ar), high flow velocities $v > 10$ cm/sec (example 18 cm/sec). Air-cooled cylindrical cell, $T_{susc.} = 1350$ K, susceptor length = 20 cm.

within 30% within every few tenths of a second. Ar and N_2 behave nearly identically and because, roughly speaking, the number of fringes is almost equal (theoretically N_2 gives about 5% more fringes), the flow patterns look very much alike too.

N_2 and Ar in a water-cooled cylindrical cell.—Similar patterns were obtained as with an air-cooled cell, but in this case only at very low flow velocities (<3 cm/sec) was the pattern stable. Above 10 cm/sec the pattern became very turbulent, although a more or less laminar part could still be discerned near the susceptor (Fig. 10 and 11). Most remarkable is that, unlike the cases with H_2 and He in a water-cooled cell, the fringes do not bend into the susceptor. Even at high velocities when the system is turbulent, a laminar layer with fringes parallel to the susceptor can be distinguished.

H_2, He, N_2, and Ar in an air-cooled rectangular cell.—In air-cooled rectangular reactor cells the same general flow phenomena are observed as with cells with a circular cross section, *i.e.*, stable flows for H_2 and He with some influence on the fringe pattern at higher flow rates (Fig. 12). Also N_2 and Ar give similar patterns as obtained with these gases in the air-cooled cylindrical cell. The sequence of photographs of Fig. 13 and 14 clearly shows how the flow pattern gradually changes due to an increase of the flow velocity from 1.5 to 15 cm/sec. At low flow velocities (1.5 cm/sec) buoyancy forces are stronger than the forces coupled with the forward motion; at 4 cm/sec the laminar layer close to the susceptor splits off, beyond 8 cm/sec two (sometimes three) rolling centers become active. These centers mark the onset of turbulent instability. At 15 cm/sec and above the system is entirely dominated by vehement turbulence although the laminar layer can still be discerned. Note the pressure effects

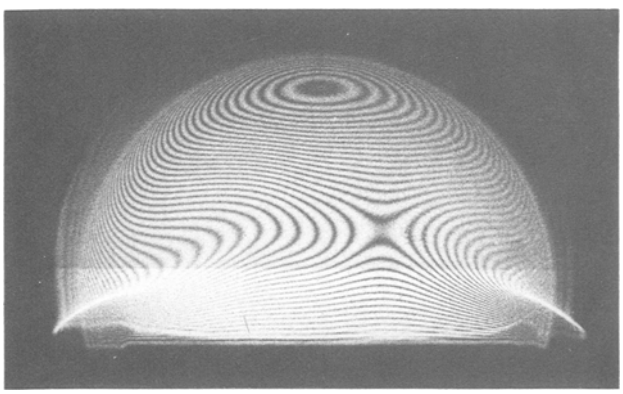

Fig. 10. N_2, water-cooled cylindrical cell, $v = 1.5$ cm/sec. $T_S = 1200$ K, $L_S = 20$ cm. Note the severe diffraction of the light due to the large density gradients.

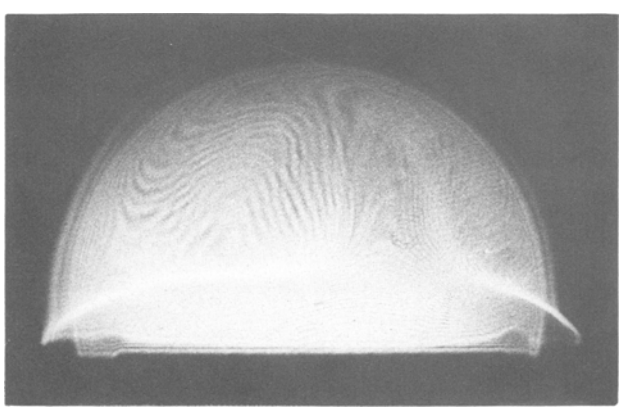

Fig. 11. N_2, water-cooled cylindrical cell $v = 15$ cm/sec. $T_S = 1200$ K, $L_S = 20$ cm.

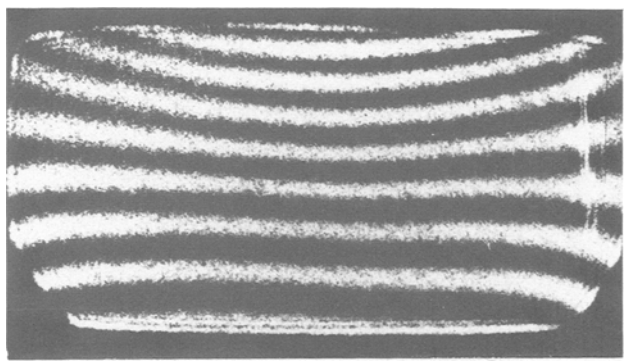

Fig. 12. H_2 (He), air-cooled rectangular cell $v = 20$ cm/sec. $T_{susc.} = 1300$ K, susc. length = 20 cm.

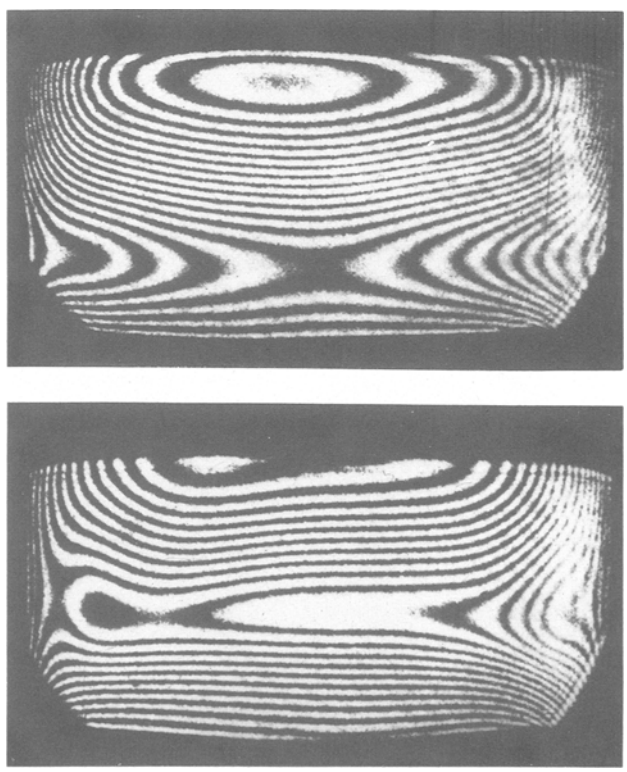

Fig. 13. N_2 (Ar), air-cooled rectangular cell, $T_{susc.} = 1350$ K, length = 20 cm. (a, top) $v = 1.5$ cm/sec; (b, bottom) $v = 4$ cm/sec.

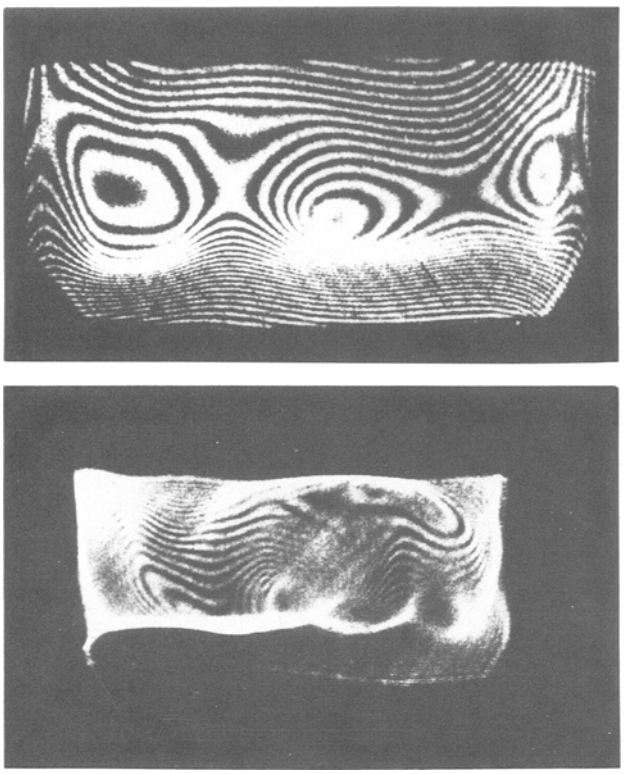

Fig. 14. N_2 air-cooled rectangular cell, T_S = 1350 K, L_S = 20 cm. (a, top) v = 8 cm/sec; (b, bottom) v = 15 cm/sec.

of the turbulent centers on the laminar layer underneath.

H_2, He, N_2, and Ar in a top-cooled rectangular cell.—For the rectangular cell that is cooled on the top-side by a water jacket, the stability in fringe pattern with H_2 and He again is comparable with water-cooled circular cells. The absence of the cooling of the side walls now gives a rather ideal fringe pattern, *i.e.*, all the fringes run almost parallel to the susceptor surface and the total number of fringes is equal to the theoretical number based on the two well-defined temperatures, *i.e.*, the temperature of the susceptor and 300 K of the water-cooled top (Fig. 15). The fringe pattern obtained at low flow velocities with N_2 and Ar for this top-cooled cell does not differ much from that observed for the air-cooled cell. However at higher flows, when the "laminar" part has split off, the fringe pattern which up to now had an "upwards" bell-like shape in the middle, suddenly flips to the inverted situation (Fig. 16). Increasing the flow rate again has the same effect as with the other cells: convection and much turbulence in the upper part, dynamic stability and more or less horizontal parallel lines in the lower part with rapidly changing variations in local thickness due to the pressure effects of the convective and turbulent rolls (Fig. 17).

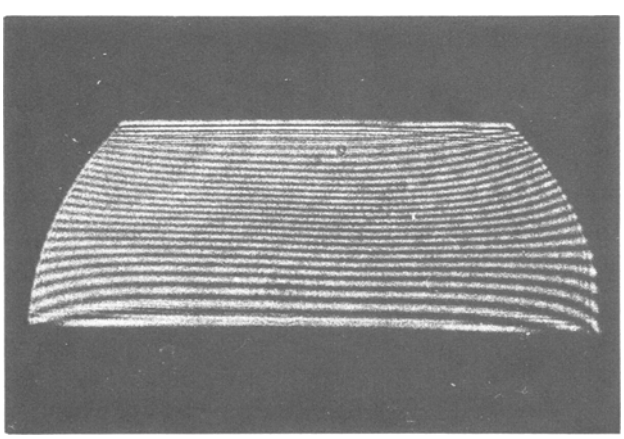

Fig. 15. H_2 (He) top-cooled rectangular cell, all flow velocities < 90 cm/sec. $T_{susc.}$ = 1130 K, susc. length = 20 cm (example v = 64 cm/sec). (The side walls of the cell are bounded by an optical diaphragm.)

Discussion

The experimental data should allow us to give an answer to the following basic questions:

1. Is the flow profile laminar or turbulent?
2. Can one distinguish a boundary layer?
3. What is the influence of cell design?
4. What is the temperature distribution?

Apart from an answer to question 4, which is given in a following paper, these questions will be discussed in this order.

Most striking of course is the difference in stability between the gases H_2 and He on the one hand and N_2 and Ar on the other. This instability may be due to three main factors which are: (*i*) instability due to turbulence, (*ii*) instability due to convection, and (*iii*) instability due to entrance effects. In the next three paragraphs the contribution of these three effects will be discussed separately.

Turbulence.—The flow through a channel, which is at a constant temperature everywhere, is characterized by its Reynolds number $\mathrm{Re} = vh\rho/\eta$ in which v[m/sec] is the mean flow rate, h the height of the channel [m], ρ the density of the gas [kg/m^3], and η its dynamic viscosity [kg/msec]. The values for η (T) and ρ (T) are plotted in Fig. 18 and 19[1] (9-11). For low Reynolds numbers the flow is laminar, for flows beyond a critical Reynolds number the flow is turbulent. The critical number for flow in a tube is 2300 (12). In Table

[1] ρ follows from the ideal gas law $\rho = M/V$ with M_{H_2} = 2.016g, M_{He} = 4.0026g, M_{N_2} = 28.0134g, M_{Ar} = 39.948g, and at 0°C V_{H_2} = 22.4321, V_{N_2} = 22.4031, V_{Ar} = 22.3901, V_{He} = 22.3961.

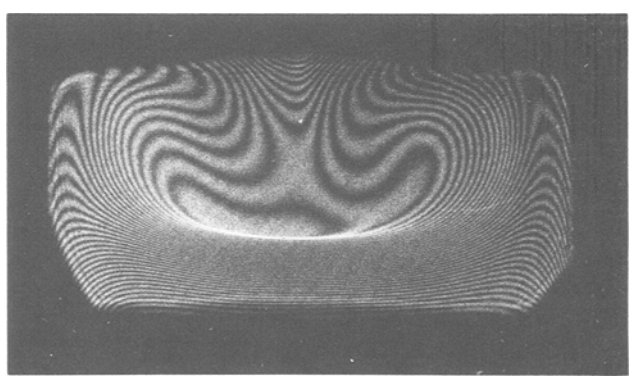

Fig. 16. N_2 (Ar), top-cooled rectangular cell, v = 10 cm/sec. $T_{susc.}$ = 1530 K, susc. length = 20 cm.

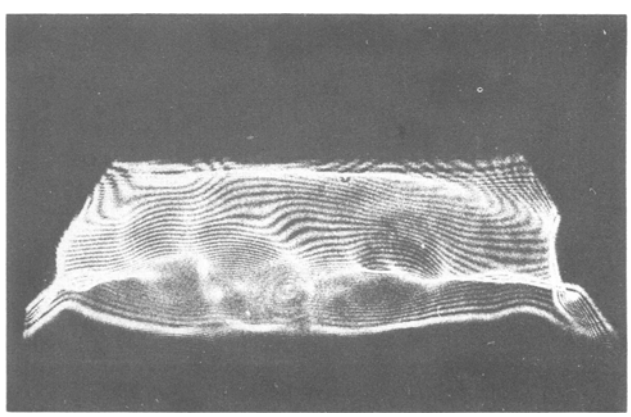

Fig. 17. N_2 (Ar), top-cooled rectangular cell v > 10 cm/sec

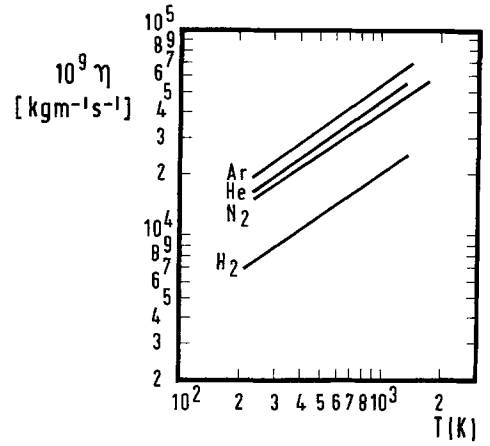

Fig. 18. Log-log plot of the viscosity of H_2, He, N_2, and Ar as a function of temperature.

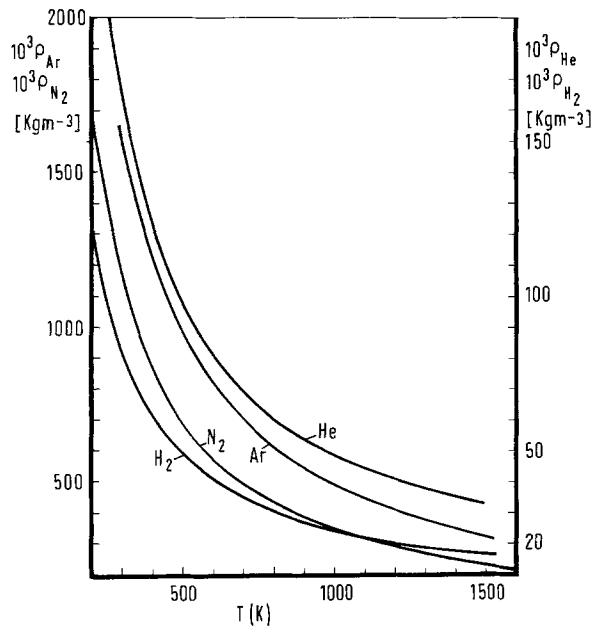

Fig. 19. Densities of H_2, He, N_2, and Ar as a function of temperature.

I the Reynolds numbers for the four gases H_2, He, N_2, and Ar are calculated for two flow rates, *viz.* 40 and 120 cm/sec and for 300, 1000, and 1400 K. A free height of 2.5 cm is taken as the value for h. One should notice that because of the temperature dependence of ρ and η, the flows stabilize at higher temperatures. From their temperature dependence it follows that the Reynolds number varies with $T^{-1.7}$.

Inspection of Table I shows that no turbulence is to be expected for all gases, with the exception of N_2 and Ar at higher flow rates (>120 cm/sec) and room temperature, where the onset of turbulence is approached. Such a situation can develop in a reactor where the incoming gas undergoes an extra acceleration due to expansion of the gas at the hot susceptor. The situation is complicated by the fact that the hottest parts of the gas also have the highest viscosity and consequently move slower. Because part of the gas expands and moves slower the colder parts of the gas stream have to move much faster in order to maintain the mean room temperature input velocity. In principle this effect is responsible for part of the phenomena observed with N_2 and Ar, as will be discussed at the end of the section "Entrance effects."

Table I. Reynolds numbers for H_2, He, N_2, and Ar; h = 2.5 cm

	40 cm/sec			120 cm/sec		
	300 K	1000 K	1400 K	300 K	1000 K	1400 K
H_2	91	12	7	274	27	21
He	82	11	6	245	33	19
N_2	639	85	50	1917	256	149
Ar	715	92	54	2146	277	161

Convection.—In the absence of a forced flow in the long direction of the cell (v = 0), a vertical flow can still be present due to buoyancy forces. These can become active when in the z-direction of the cell a negative temperature gradient is present. This is called convection. In the reactor cell where the top is cooled with water (300 K), or air (800 K) and the bottom is heated to 1400 K, such an inverted temperature field exists (Fig. 20). Convection will occur when the Rayleigh number[2] exceeds the value 1707 (13, 14). The Rayleigh number is given by

$$\mathrm{Ra} = \frac{\alpha g c_p \rho^2 h^3 \Delta T}{\eta \kappa}$$

where α = coefficient of thermal expansion = $(1/T)$, g = gravitational acceleration (9.81 msec^{-2}), ρ = density [kg m^{-3}], h = free height above susceptor [m], $\Delta T = T_{bottom} - T_{top}$, η = dynamic viscosity [kgm^{-1} sec^{-1}], κ = thermal conductivity [Jm^{-1} sec^{-1} K^{-1}], and c_p = specific heat [J kg^{-1} K^{-1}].

Values for c_p and κ are collected in Fig. 21 and 22 and Table II. They were taken from Ref. (16)-(19). Using these values, the Rayleigh numbers for the four gases are calculated for three susceptor temperatures, *viz.* 500, 1000, and 1400 K and a constant value for the temperature at the top of the cell (300 K). The free height h is again taken as 2.5 cm. The values are collected in Table III. From this table it is evident that the flows of N_2 and Ar are highly unstable and in fact will be dominated by convection; H_2 and He on the other hand, especially at high temperatures, are resistant to convective motions. Note that the Rayleigh number varies with $T^{4.4}$ ($\alpha \propto T^{-1}$, $\eta \propto T^{0.7}$, $\kappa \propto T^{0.7}$, $\rho \propto T^{-1}$, $c_p \cong$ constant), so that also in this case stabilization occurs at higher temperatures. The conclusion is that there will be no convection for H_2 and He but that flows of Ar and N_2 will be highly convective in epitaxial reactor cells, as observed in the experiments.

Entrance effects.—Up to now it was assumed that the flow and temperature profiles were fully developed from the onset of the susceptor. However the flows

[2] In heat transfer theory, instead of the Rayleigh number, often the Grashof number G is used (15). The relation between these numbers is given by G = Ra/P where P is the Prandtl number $\eta c_p/\kappa$, which number for gases is about 0.7 and almost independent of temperature over the temperature range 300-1500 K.

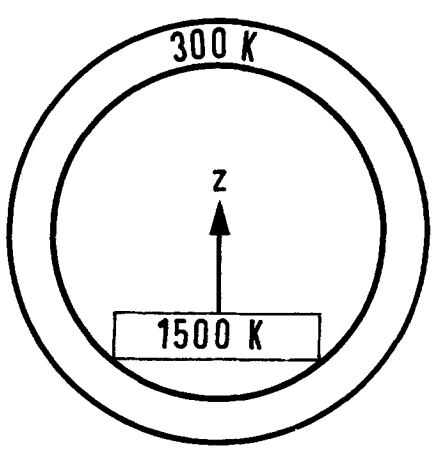

Fig. 20. Cross section of water-cooled cylindrical reactor cell. Convective instability due to inverted temperature situation.

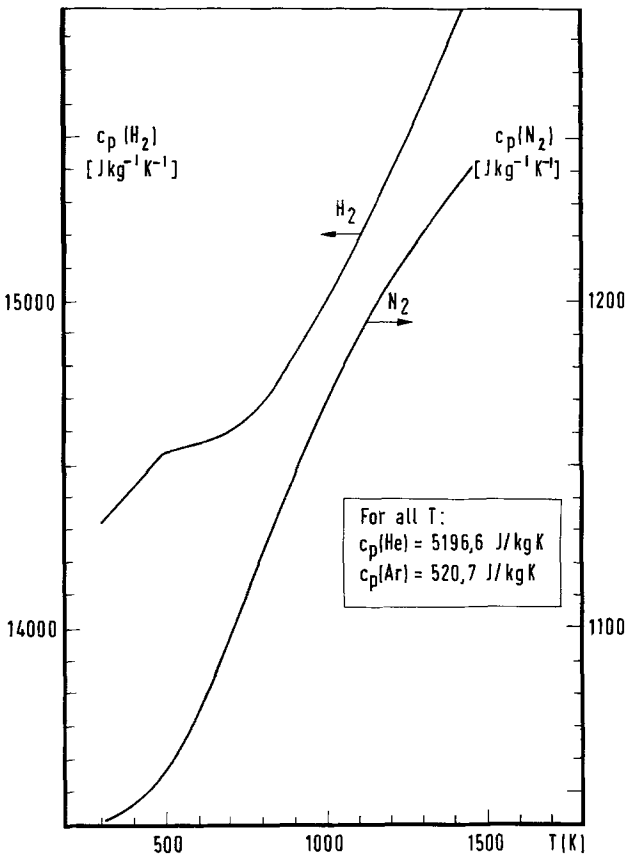

Fig. 21. Specific heat values of H_2, He, N_2, and Ar as a function of temperature.

need some macroscopic distance to develop their profiles (Fig. 23). According to Schlichting (20), flow in a channel with height h is fully developed beyond

$$x = 0.04 \frac{h^2 v\rho}{\eta} = 0.04h\,\mathrm{Re}$$

This entrance length (in cm) is calculated for two velocities, *viz.* 10 and 40 cm/sec and for 300, 1000, and 1400 K (Table IV).

It is clear that for H_2 and He, especially at low flow rates, reasonably well-developed flows are present over a good part of the susceptor. However for N_2 and Ar over a good deal or even over the complete length of the susceptor, the flow is undeveloped and will possess the properties of the gas that enters the

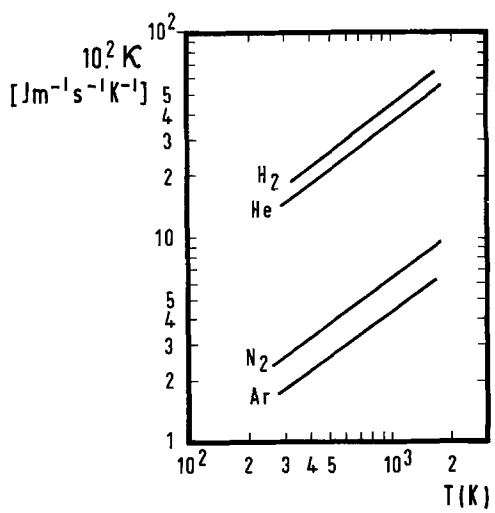

Fig. 22. Log-log plot of the thermal conductivity of H_2, He, N_2, and Ar as a function of temperature.

Table II.

	300 K				500 K			
	c_p	$10^3\rho$	$10^6\eta$	$10^6\kappa$	c_p	$10^3\rho$	$10^6\eta$	$10^6\kappa$
H_2	14315.5	81.80	8.96	180	14524	49.08	12.6	259
He	5196.6	162.6	19.87	149.9	5196.6	97.4	28.06	213
N_2	1040.2	1138	17.81	25.98	1056.6	682.8	25.59	38.4
Ar	520.7	1623.6	22.7	17.7	520.7	974	33.2	26.6
	1000 K				1400 K			
	c_p	$10^3\rho$	$10^6\eta$	$10^3\kappa$	c_p	$10^3\rho$	$10^6\eta$	$10^3\kappa$
H_2	14990	24.53	20.13	432	15784	17.53	25.0	560
He	5196.6	48.7	44.6	360	5196.6	34.8	55.0	460
N_2	1168.0	341.4	40.0	62.6	1233.3	243.8	49.0	78.5
Ar	520.7	487	52.8	42.9	520.7	347.9	65.0	52.6

c_p in [Jkg^{-1} K^{-1}], ρ in [kg m^{-3}], η in [kg m^{-1} sec^{-1}], κ in [Jm^{-1} sec^{-1} K^{-1}].

Table III. Rayleigh numbers for H_2, He, N_2, and Ar; h = 2.5 cm

	500 K	1000 K	1400 K
H_2	657	111	42
He	506	82	30
N_2	30736	5833	2295
Ar	34295	5850	2220

Table IV. Entrance lengths in cm for the development of the flow profiles of H_2, He, N_2, and Ar using h = 2.5 cm. Thermal entrance regions are 7 × longer

	300 K		1000 K		1400 K	
	10 cm/sec	40 cm/sec	10 cm/sec	40 cm/sec	10 cm/sec	40 cm/sec
H_2	2.3	9.1	0.3	1.2	0.2	0.7
He	2.1	8.2	0.3	1.1	0.2	0.6
N_2	16.0	63.9	2.1	8.5	1.3	5.0
Ar	17.9	71.5	2.3	9.2	1.4	5.4

cell, especially in the colder bulk part of the gas stream.

Besides the flow which has to develop, the temperature profile also has to achieve its proper profile (Fig. 24). For this development Hwang and Cheng (21) deduced a necessary length of

$$x = 0.28 \frac{h^2 v\rho}{\eta} = 0.28h\,\mathrm{Re}$$

i.e., the thermal entrance length is 7 times longer than the entrance length for the flow. This means that also for H_2 and He above v = 10 cm/sec no well-developed temperature profiles can be expected in the low temperature parts of the gas stream. Such high values for the theoretical entrance length are surprising, but Kamotani and Ostrach (22) experimentally confirmed the theoretically deduced entrance length of Hwang and Cheng. In addition, in a forthcoming paper it will be shown that the temperature profile measurements in

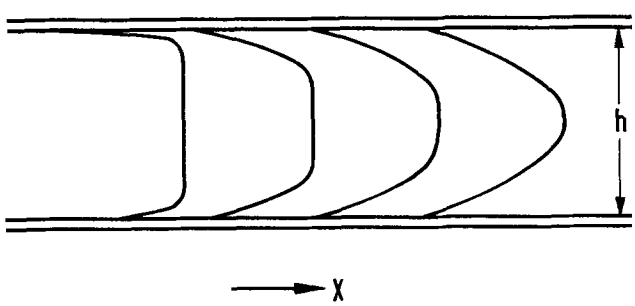

Fig. 23. Development of flow profiles in a channel. Beyond x = 0.04h Re the flow is fully developed.

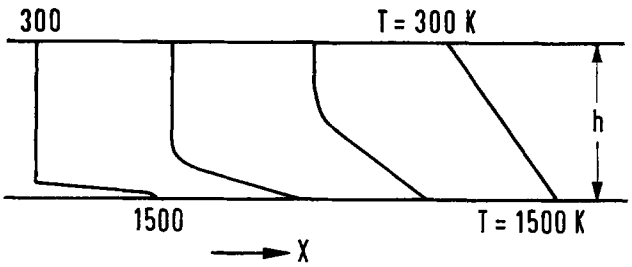

Fig. 24. Development of the temperature profile in a channel. The temperature profile is fully developed beyond $x = 0.28h$ Re, i.e., the thermal entrance length is 7× the entrance length for the flow.

the reactor cells for H_2, obtained by our interference holography experiments are in agreement with these ideas. A linear temperature profile is obtained for H_2 at 9.5 cm/sec, which profile becomes more and more curved at higher flow rates, indicating the increasing effect of the thermal entrance length.

After having considered the possibilities of turbulence, convection, and entrance effects, it becomes clear that H_2 and He indeed are expected to give a stable and laminar flow at all velocities, but that there is a possibility that their temperature profiles for $v > 10$ cm/sec are not fully developed. For N_2 and Ar no intrinsic turbulence is to be expected either, at least not at velocities lower than 120 cm/sec but there is (*i*) a very strong entrance effect (*i.e.*, when the incoming gas is turbulent it will keep its turbulence along a good deal of the susceptor), and (*ii*) a convective instability. The result is that at flow velocities above 4 cm/sec the entrance effect will be high (strong turbulence due to the incoming gas) whereas at flows < 4 cm/sec the pattern will be dominated by convection. This indeed is observed by interference holography. However, the breaking up of the flow of N_2 or Ar into two parts is not immediately obvious from theory. It looks as if the flow creates its own favorable situation. Apparently a thin (8 mm) laminar layer together with the turbulent part above it, is more attractive energetically than a complete turbulent system. The stability of the thin laminar layer can be understood in the following way. From Table IV it follows that at high temperatures the flow and temperature profiles are about 10 times sooner developed than at lower temperatures, so the entrance effects are small for this layer. In these hotter parts of the gas stream no turbulence will be present either (Table I), whereas no convection can be expected in such a thin layer of 8 mm, because the Rayleigh values in Table III will be reduced by about a factor 30 due to the h^3 dependency. This accounts for the stability of the laminar layer just above the susceptor. For the bulk stream of the gas these arguments do not hold and its character remains turbulent.

It was attempted to observe the flow pattern lateral of the cell to get an impression as to whether the laminar part was equal in thickness from the beginning to the end of the susceptor. These experiments failed, however, because of the small number of fringes and the severe disturbance of the holographic pictures by air convection outside the optical side windows.

An answer to the second question, *i.e.*, the existence of a boundary layer for the flow is more difficult to give. For H_2 and He, where the flow readily achieves its parabolic profile within a few centimeters of the leading edge of the susceptor, no strict boundary layer is present in the sense of deviations of the normal profile. Because in the reactor cell the final velocity profile is almost a parabola (in fact it is an asymmetric parabola with its maximum shifted to the low temperature side), one can speak of an effective boundary layer thickness for the flow of $\frac{1}{2}h$ in this case, assuming that in a rectangular cell the lines of maximum throughput, *i.e.*, the main mass flux, will predominantly coincide with the lines of maximum velocity. (For a cylindrical cell this need not be true, because for the calculation of the main mass flux the velocity must be multiplied by its r-dependent surface area.) When the temperature profile has completely developed within the first centimeters of the susceptor, no thermal boundary layer is present either. This is the case for H_2 and He at $v < 10$ cm/sec; above this value undeveloped temperature profiles are present in H_2 and He, and a thermal boundary layer can be discerned.

For N_2 and Ar a boundary layer will always be present. For flow rates above 4 cm/sec the flow and temperature boundary layers are equivalent, in this case being equal to the thickness of the split off layer. It must be noted that, especially at higher flow rates, locally the boundary layer is disturbed for these gases, only the mean thickness is constant. It also is not certain that the thickness of the laminar layer is constant from the beginning to the end of the susceptor.

Boundary layer thicknesses are important when epitaxial layers are grown in the diffusion-limited regime. Here the growth rate is proportional to D/δ, where D is the diffusion coefficient of the component in the carrier gas and δ is the thickness of the concentration boundary layer. When it is assumed that the concentration and the flow boundary layers coincide then it follows from this study that for rectangular cells in H_2 and He $\delta \cong \frac{1}{2}h$, whereas for Ar and N_2 $\delta \cong 0.8$ cm. This observed difference in the values of δ in combination with the known (23) differences in the diffusion coefficients of the chemically active components in the four carrier gases, offers the opportunity to test calculated values of D/δ. This can best be verified for the growth of silicon in He and Ar because these carrier gases are not involved in the chemistry of the deposition process, as is H_2 and for some reactions also N_2. A prerequisite to such an experiment is, of course, that for He the flow and temperature profiles must be fully developed.

Sparrow and co-workers (24) have suggested the use of the Gr/Re^2 (Gr = Grashof number) ratio for characterization of the flow. Forced flow is dominant for $Gr/Re^2 < 0.3$, mixed flow between 0.3 and 16, and above 16 free convection dominates. No such correlation was observed in our experiments. All calculated values of Gr/Re^2 are equal for all gases at a given temperature. For instance, no characteristic difference is noticed between the values for H_2 and N_2, whereas hydrogen gives a stable laminar, but nitrogen a highly unstable and convective flow. So it appears that the ratio Gr/Re^2 is not a good measure for the characterization of the flow. Berkman, Ban, and Goldsmith (25) have given an analysis of the gas flow dynamics in a horizontal reactor based on the observations of Ban (3, 4). This analysis basically accepts the boundary layer model as treated in various books on hydrodynamics. The present experimental data make it clear that especially for H_2 and He in well-developed profiles, no boundary layer is present in the sense accepted by Berkman, Ban, and Goldsmith. For N_2 and Ar, and only in a very narrow velocity range, is a split off boundary layer observed. However the width of this layer mathematically is not governed by the boundary layer theories as used by these authors.

The influence of cell design (to give an answer to the third question) on the flow and temperature profiles is demonstrated by the differences between air-cooled and water-cooled cells (Fig. 4, 5, and 6). Three characteristic differences come about: (*i*) At the same

high flow velocity a cold gas finger is only present in the air-cooled cells; (*ii*) the temperature of the quartz wall for the air-cooled cell is between 600 and 900 K (part II); (*iii*) water-cooling of the side walls gives a serious temperature gradient across the susceptor for H_2 and He. The cold gas finger points to a much higher flow velocity in this part of the air-cooled cell than in the corresponding region of the water-cooled cell. The reason is an extra volume expansion of 2 or 3 times at the hot walls of the air-cooled cell together with a corresponding higher viscosity of the gas at these walls. The effect of the latter is that the gas has a lower than normal velocity at the wall and because the mean velocity of the gas is fixed, as determined by the input flow; the core velocity must go up to maintain the same mean velocity. The consequence of this is a more severe entrance effect which shows up as a cold finger. The difference between H_2 (He) and Ar (N_2) regarding the temperature gradient across the susceptor for water-cooled cells (Fig. 6 and 10) is recognized as being due to the much higher thermal conductivities of H_2 and He as compared to Ar and N_2. With N_2 (Ar) the heat cannot be dissipated fast enough by conduction and the profile across the susceptor remains flat.

Reactor Cell Recommendations

From the experimental data and the analysis given above it is possible to formulate the requirements for an optimized reactor cell, *viz.* (*i*) no temperature gradient across the susceptor, (*ii*) stable laminar flows, and (*iii*) well-developed temperature and flow profiles. These requirements can be met by taking a rectangular cell with water cooling at its top only. The cell should have a small free height, of about 1 cm for instance, to guarentee well-developed flow and temperature profiles. It should also be provided with a long entrance piece at equal level to the susceptor and if possible provided with preheaters (Fig. 25).

For growth situations it is recommended that the silicon wafers be kept some distance away from the sidewalls. The reason is that these sidewalls will have some effect on the normal flow profile, while the temperature will also be slightly affected. A distance equal to the free height probably will be sufficient. For very accurate epitaxial deposition it appears desirable to work in a stable well-developed laminar flow. This implies that only H_2 and He are useful as carrier gases. Their flow profile is known, and provided the gas is preheated, also the temperature profile is fixed. This situation lends itself for a comparison between experiment and theory on crystal growth from the vapor phase.

More uncertainties are present when N_2 or Ar is used, especially because of the unknown variation of the boundary layer thickness in the length direction of the susceptor. However the combination of a laminar split off layer with a turbulent layer above it may be of advantage for those crystal growth processes where the gas phase becomes quickly depleted. In these cases the turbulent part may (by its low temperature, high velocity, and well mixing) provide a phase with a homogeneous concentration of constituents all over the length of the split off layer. The MOCVD of GaAs may be a good example of such a system.

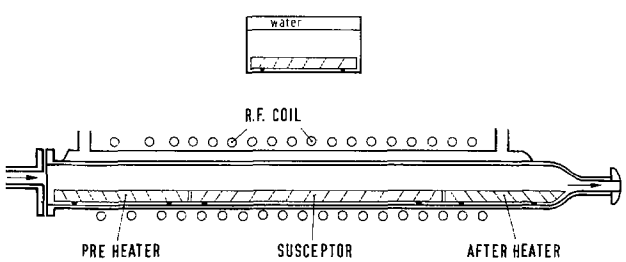

Fig. 25. Ideal reactor cell: top-cooled rectangular cell with small free height ≅ 1 cm, long entrance piece at equal height as the susceptor. When this entrance piece is made of carbon it can also act as a preheater. The heater after the susceptor reduces temperature gradients along the susceptor. Dead volumes are kept as small as possible.

Conclusion

The method of interference holography has given valuable information on the flow patterns of the four carrier gases H_2, N_2, He, and Ar. The main effect which one should be aware of in reactor cells is the entrance effect. Especially for N_2 and Ar, this effect is responsible for unstable flow patterns, *i.e.*, a stable laminar part near the susceptor and a turbulent part above it.

H_2 and He are always stable, but the temperature profile is not completely developed at high flow rates.

In general all effects can be reduced considerably by a proper design of the reactor, *i.e.*, long inlet lengths, combined with a low free height above the susceptor and top cooling only.

Acknowledgments

Many co-workers have given excellent contributions to this research work. My sincere thanks are especially due to Jan Wanrooy, Paul Bunk, Ad van der Ven, Guus Verheyen, and Bauke Leyenaar for their fruitful cooperation.

The author also gratefully acknowledges the stimulation and interest of Prof. Jan Bloem during this work.

Manuscript submitted March 16, 1981; revised manuscript received July 15, 1981.

Any discussion of this paper will appear in a Discussion Section to be published in the December 1982 JOURNAL. All discussions for the December 1982 Discussion Section should be submitted by Aug. 1, 1982.

Publication costs of this article were assisted by Catholic University.

REFERENCES

1. F. C. Eversteyn, P. J. W. Severin, C. H. J. v.d. Brekel, and H. L. Peek, *This Journal*, **117**, 925 (1970).
2. F. C. Eversteyn, *Philips Res. Rep.*, **26**, 134 (1971).
3. V. S. Ban and S. L. Gilbert, *J. Crystal Growth*, **31**, 284 (1975).
4. V. S. Ban, *This Journal*, **125**, 317 (1978).
5. T. O. Sedgwick, J. E. Smith, Jr., R. Ghez, and M. E. Cowher, *J. Crystal Growth*, **31**, 264 (1975).
6. L. J. Giling, Extended Abstract, pp. 17-22, "Int'l. Conf. on Crystal Growth," Boston (1977).
7. R. J. Collier, C. B. Burckhardt, and L. H. Lin, "Optical Holography," Academic Press, New York (1971).
8. J. B. DeVelis, "Theory and Applications of Holography," Addison-Wesley Publ. Co., London (1967).
9. Landolt Börnstein 6. Auflage, "Zahlenwerte und Funktionen," II. Band, 5. Teil Bandteil a, Transportphänomene I, pp. 13-26. Springer Verlag, Berlin, New York (1969).
10. R. C. Weast, "Handbook of Chemistry and Physics," 52nd ed., p. F43. The Chemical Rubber Co., Cleveland (1970).
11. E. A. Mason and W. E. Rice, *J. Chem. Phys.*, **22**, 522 (1954).
12. H. Schlichting, "Boundary-Layer Theory," 6th ed., p. 432, McGraw-Hill, New York (1968).
13. H. H. Sogin and H. A. Thompson, "Proc. 5th Symposium on Thermophysical Properties," Newton, Mass., Oct. 1970.
14. B. J. Curtis and J. P. Dismukes, *J. Crystal Growth*, **17**, 128 (1972).
15. F. Kreith, "Principles of Heat Transfer," 2nd ed., Int. Textbook Co., Scranton, PA (1965).
16. D. R. Stuhl and H. Prophet, JANAF Thermochemi-

cal Tables NSRDS-NBS 37, 2nd ed., U.S. Government Printing Office, Washington, D.C. (1971).
17. Landolt Börnstein 6. Auflage, "Zahlenwerte und Funktionen," VI. Band, 4. Teil, Warmetechnik, Bandteil b, pp. 588-590, Springer Verlag, Berlin, New York (1972).
18. Landolt Börnstein, 6. Auflage, "Zahlenwerte und Funktionen," II. Band, 5. Teil, Bandteil b, Transport-phänomene II, Kinetik, pp. 45-48, Springer Verlag, Berlin, New York (1968).
19. R. C. Weast, "Handbook of Chemistry and Physics," 52nd ed., p. E3, The Chemical Rubber Co., Cleveland (1970).
20. H. Schlichting, "Boundary-Layer Theory," 6th ed., pp. 177-178, McGraw-Hill, New York (1968).
21. G. J. Hwang and K. C. Cheng, *J. Heat Transfer, Trans. ASME*, **95**, 72 (1973).
22. Y. Kamotani and S. Ostrach, *ibid.*, **98**, 62 (1976).
23. R. H. Perry, C. H. Chilton, and S. D. Kirckpatrick, "Perry's Chemical Engineer's Handbook," Section 14-20, 4th ed., McGraw-Hill, New York (1969).
24. E. M. Sparrow, R. Eichhorn, and J. L. Gregg, *Phys. Fluids*, **2**, 319 (1959).
25. S. Berkman, V. S. Ban, and N. Goldsmith, in "Heteroepitaxial Semiconductors for Electronic Devices," G. W. Cullen and C. C. Wang, Editors, Springer, New York (1978).

The Enhanced Diffusion of Arsenic and Phosphorus in Silicon by Thermal Oxidation

Yutaka Ishikawa, Yasuharu Sakina, Hitoshi Tanaka, Satoru Matsumoto, and Tatsuya Niimi

Department of Electrical Engineering, Keio University, Hiyoshi, Yokohama 223, Japan

ABSTRACT

It was investigated and found that the enhanced diffusion of arsenic and phosphorus in silicon by thermal oxidation is dependent on the crystal orientation of a substrate, diffusion temperature, and time. Impurities are prediffused into a silicon substrate from impurity-silica film, and then subjected to a drive-in diffusion in oxidizing (dry O_2) and inert (dry N_2) atmosphere. Diffusion coefficients are determined by adopting best fitted parameters in the numerical simulation of the experiments. The diffusion coefficients of arsenic and phosphorus are enhanced by thermal oxidation of silicon. This enhancement measured in (100) silicon is greater than that in (111) silicon. The diffusion coefficients obtained in oxidizing atmosphere can be expressed as a function of diffusion temperature and time. From the form of this equation, it is considered that arsenic and phosphorus diffuse by the dual mechanism (vacancy and interstitialcy mechanism). The enhancement increases in order of arsenic, phosphorus, and boron.

Oxidation-enhanced diffusion of group III and group V elements in silicon has been studied extensively for the fundamental understanding of device fabrication (1-10). Antoniadis *et al.* (5) reported that the enhancement in boron diffusion in oxidizing atmosphere depended on the crystal orientation of silicon substrate as well as diffusion temperature. They also reported the oxidation-enhanced diffusion of arsenic and phosphorus in silicon (6), in which they did not refer to a relation between the crystal orientation and the enhanced diffusion. Moreover, they suggested that the diffusion coefficients of these three impurities in silicon depended on diffusion time in oxidizing atmosphere (5, 6). However, they proposed no definite data about it.

When an impurity of high concentration is diffused into a substrate in oxidizing atmosphere, the two different causes of the anomalous behavior in diffusion, which are due to the enhanced diffusion by oxidation and the high concentration effects of the impurity on the diffusion profiles, will be present simultaneously and they will make analysis of the experimental results difficult. The separation of these two causes has not been considered fully in most reports on the oxidation-enhanced diffusion.

In this paper, with the intention of separating the two causes of the anomalous diffusion, arsenic and phosphorus are diffused into (100) and (111) silicon substrates under different temperatures and times in both oxidizing and inert atmosphere under intrinsic diffusion conditions. Here we define the intrinsic diffusion conditions as follows, that is, the concentration of diffused impurity in silicon is lower than the intrinsic carrier concentration at the process temperature, and also define the intrinsic diffusion coefficient as the diffusion coefficient obtained under the intrinsic diffusion conditions. It is made clear by the determination of the diffusion coefficients of the impurities by the numerical simulation that the enhanced diffusion by oxidation is dependent on the crystal orientation of the silicon substrate, diffusion temperature, and diffusion time. Moreover, the oxidation-enhanced diffusion of boron is investigated in order to compare the enhancement in boron diffusion with that in the diffusion of arsenic and phosphorus. The diffusion mechanism of these three impurities in oxidizing atmosphere is discussed on the basis of the experimental results.

Key words: oxidation, diffusion, enhancement, semiconductor.

Experimental

The substrates used were Czochralski-grown, p-type and n-type dislocation-free, (100) and (111) oriented silicon wafers of resistivity 1-6 Ω-cm. Arsenic or phosphorus-silica film was attached onto the substrates, using a spinner. The thickness of the film was about 1500Å. These substrates were baked at 200°C for 20 min in dry N_2. Then the impurity contained in the film was prediffused into the silicon substrate at 1050°C for 20-180 min. After the film was removed from the surface of the substrate by dilute HF solution, the substrate was subjected to a drive-in diffusion at 950°-1150°C in both dry O_2 and dry N_2. Drive-in diffusions were carried out for the different diffusion times at a certain diffusion temperature. For drive-in diffusions in dry N_2, the silicon surfaces were covered with a nondoped silicon dioxide film to avoid out-diffusion of the impurity. Boron diffusion was also carried out under the condition of several kinds of the combination of diffusion temperature and time through the same process as for arsenic and phosphorus.

Impurity concentrations in the substrates were determined after the prediffusion and the drive-in diffusion. The sheet resistivities were measured by a four-point probe method. The successive removal of a thin